DOI 10.34658/jacs.2018.26.1.87-104

JOURNAL OF APPLIED
COMPUTER SCIENCE
Vol. 26 No. 1 (2018), pp. 87-104

Robust Two-View Reconstruction Procedure for Geometrical Model Retrieving

Jakub Walczak[1], Adam Wojciechowski[1]

[1]*Lodz University of Technology*
Institute of Information Technology
ul. Wólczańska 215, 90-924 Łódź, Poland
`http://it.p.lodz.pl/`

Abstract. *In this paper we present the enhancement of the standard two-view reconstruction procedure. An ordinary approach assumes determination of points' correspondences followed by projection matrix estimation, to finally refine results with bundle adjustment taking as a cost function reprojection error. Our contribution is realized in two manners: introducing an additional step of outliers rejection, changing cost function of bundle adjustment process to Relative Reprojection Error (ϵ^R) and applying central difference as a method for Jacobian matrix approximation. Tests revealed gain in average ϵ^R with lower variance, for confidence level of 0.95. Besides accuracy improvement, the suggested modifications supply the final result in the time virtually independent on initial object's complexity and, in most cases, shorter than the standard approach.*
Keywords: *3D reconstruction, epipolar geometry, photogrammetry, model refinement.*

1. Introduction

Direct analysis of data present in an image is valuable for many purposes, however, it does not regard spatial relationships, barely depicted with a projec-

tion. In many problems, especially within robotics domain, possession of a three-dimensional model, even reasonably simplified, might be advantageous and could make further processing more accurate or reliable. But here an other problem arises, namely knowing the computer model of a scene is difficult or, very often, impossible in advance. Thus the procedure of Structure from Motion (SfM) came into being. It may be thought of as a process of building a 3D model of a scene by reasoning from a range of available clues, for instance: parallax effect or shadows distribution. Current taxonomy of this domain introduced two groups of reconstruction methods, divided with respect to the role illumination plays in the reconstruction process [1]. These groups are constituted by *active* and *passive* techniques. The active ones apply lightning patterns to generate actively depth clues. Structured Light [2, 3] methods or, its more accurate version, Laser Line Scan [4, 5] are cases in point. On the other hand we have passive techniques making use of information captured with an ordinary camera. This usually uses projections from different viewpoints.

Undoubtedly, active methods solve many problems of simple multiple-view reconstruction: correspondence issue, complex texture influence or poorer accuracy [6] just to name a few, however, they require either virtually laboratory acquisition conditions or expensive tools designed for far remote sensing. That is why structured light and its derivatives have to be rejected in some cases.

Contrary to active methods, multiple-view reconstruction, based on photogrammetry, makes use just of images correspondence captured with an ordinary camera.

2. Related works

Multiple-view reconstruction follows usually a standard sequence of procedures aiming in creation some sort of model. The algorithm is depicted in the Figure 1 [1].

Having two frames F1 and F2 provided (stage a), SURF features (our keypoints) are extracted and aggregated into two vectors $\mathbf{x} =< x_1, x_2, x_3, ..., x_n >$ and $\mathbf{x}' =< x'_1, x'_2, x'_3, ..., x'_m >$ (stage b), where n and m are number of features in frame F1 and F2 respectively. The correspondences between respective features $< x_1, x_2, x_3, ..., x_n >$ and $< x'_1, x'_2, x'_3, ..., x'_m >$ may be then found (stage c). Usually for this process RANSAC method is employed so as to boost accuracy of matching [7]. Having collected information about respective features' locations in both frames, and bearing in mind intrinsic camera parameters $\mathbf{K}$ (Eq. 1) responsible

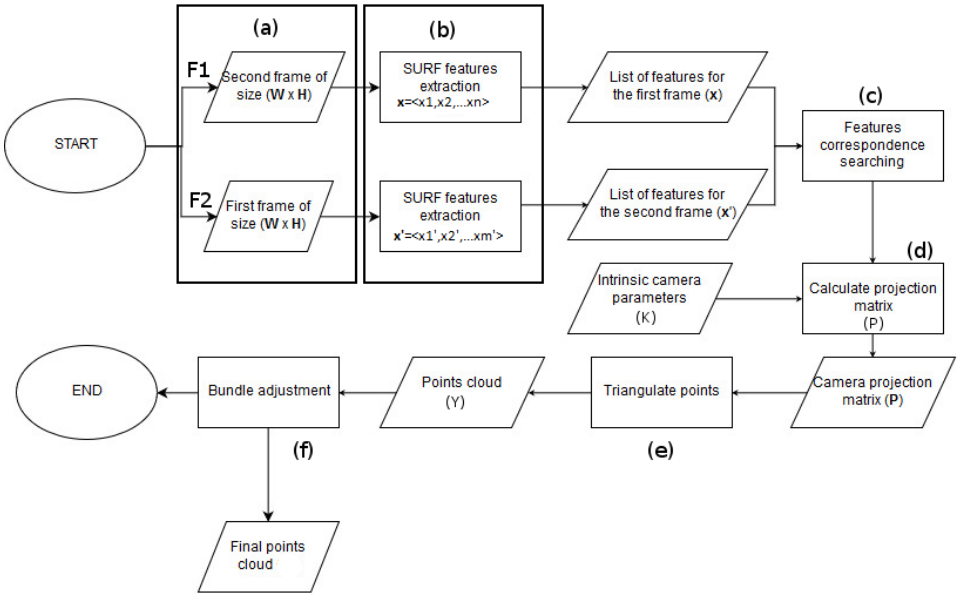

Figure 1: Basic flow of scene reconstruction procedures Source: Own work

for transforming camera coordinates into image coordinates, one can approximate the essential matrix **E** (Eq. 2). The essential matrix is generally defined as 3 [7]. The illustration of the idea of two-view reconstruction is presented in the Figure 2, where capital Y_1 is a 3D point, x_1 and x_1' are projections of the point Y_1 onto views $F1$ and $F2$ respectively, O_1 and O_2 are cameras' centers.

$$\mathbf{K} = \begin{bmatrix} f_x & s & c_x \\ 0 & f_y & c_y \\ 0 & 0 & 1 \end{bmatrix} \tag{1}$$

$$\mathbf{E} = \begin{bmatrix} e_1 & e_2 & e_3 \\ e_4 & e_5 & e_6 \\ e_7 & e_8 & e_9 \end{bmatrix} \tag{2}$$

$$\mathbf{x_i}^T \mathbf{E} \mathbf{x_i'} = 0 \ \text{ for correspondences } \ x_i \leftrightarrow x_i' \tag{3}$$

On the grounds of estimated matrix **E** one ought to solve projection ambiguity (choosing the solution out of four possibilities), taking into consideration that the

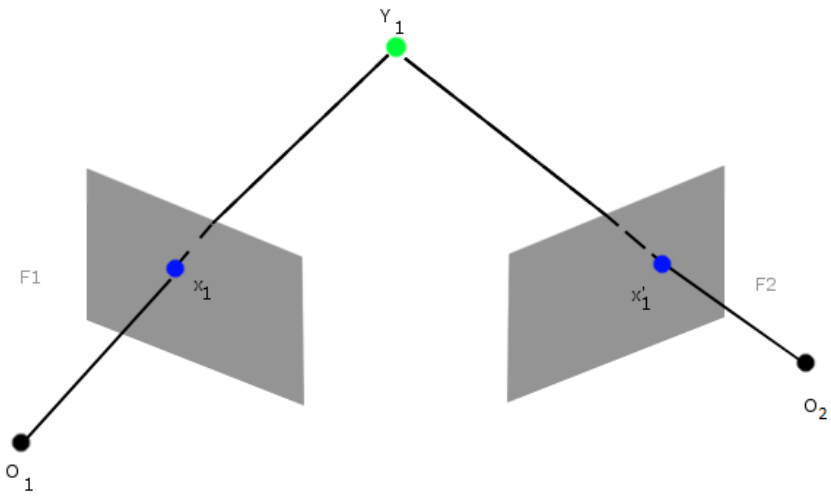

Figure 2: Idea of two-view reconstruction. Source: Own work

only real projection matrix **P** (Eq. 4) describes 3D points being in front of both cameras (stage d).

$$\mathbf{P} = [\mathbf{R} \mid \mathbf{t}] = \begin{bmatrix} r_1 & r_2 & r_3 & t_x \\ r_4 & r_5 & r_6 & t_y \\ r_7 & r_8 & r_9 & t_z \end{bmatrix} \tag{4}$$

where **P** is denoted as concatenation of a rotation matrix **R** and a translation vector **t**. Formula is valid for correspondences in image coordinates.

Now, let us describe the process of decomposition an essential matrix **E** into four different variants of the projection matrix of the second camera $\mathbf{P_2}$, assuming that projection matrix of the first camera is $\mathbf{P_1} = [\mathbf{I} \mid \mathbf{0}]$. Following this, one need to decompose an essential matrix E into multiplication of a skew-symmetric matrix **S** and a rotation matrix **R**. Supposing SVD (Singular Value Decomposition) of a matrix **E** is of the form $E = Udiag(1, 1, 0)V^T$ and taking as a goal decomposition, such that $\mathbf{E} = RS$, we may found two results (Eq. 5, 6).

$$E = R_1 S_1 = \underbrace{(U \begin{bmatrix} 0 & 1 & 0 \\ -1 & 0 & 0 \\ 0 & 0 & 1 \end{bmatrix} V^T)}_{R_1} \underbrace{(V \begin{bmatrix} 0 & -1 & 0 \\ 1 & 0 & 0 \\ 0 & 0 & 0 \end{bmatrix} V^T)}_{S_1} \tag{5}$$

$$E = R_2 S_2 = \underbrace{(U \begin{bmatrix} 0 & 1 & 0 \\ -1 & 0 & 0 \\ 0 & 0 & 1 \end{bmatrix}^T V^T)}_{R_2} \underbrace{(V \begin{bmatrix} 0 & -1 & 0 \\ 1 & 0 & 0 \\ 0 & 0 & 0 \end{bmatrix} V^T)}_{S_2} \tag{6}$$

Orthogonality and value of determinant equal to 1 can be easily proved for a rotation matrix. Now, a vector **t** needs to be extracted from **S** such that $\mathbf{S} = [t]_\times$. Following this, we may derived that **t** lies in the null space of **E** (Eq. 7)

$$Et = RSt = R[t]_\times t = 0 \tag{7}$$

From this we may obtain translation vector **t** as a last column of the matrix **U** (see SVD of matrix **E**). Because **t** is in the null space of **E** so are all vectors of the form $\lambda\mathbf{t}$ (for any scalar $\lambda \in \mathbb{R}$), what states for different scales of the vector **t**. Since, the scale cannot be uniquely determined, we need to consider solely a sign. That is reason why we may formulate four different solutions of projection matrix $\mathbf{P_2}$ (Eq. 8-11).

$$P_2 = [R_1 \mid t] \tag{8}$$

$$P_2 = [R_1 \mid -t] \tag{9}$$

$$P_2 = [R_2 \mid t] \tag{10}$$

$$P_2 = [R_2 \mid -t] \tag{11}$$

Knowing locations of points' projections (x_i,x_i') and having relative move between cameras (encoded in projection matrix), 3D points' counterparts $\{y_1, y_2, ..., y_l\} \in \mathbf{Y}$ could be triangulated (stage e). Certainly, the estimated solution may leave something to be desired. This is wreaked by noise presence (during taking images or key-points detection), error of numerical calculations and features mismatching. To overcome it somehow, non-linear optimization process, called *bundle adjustment*, is often introduced. It usually makes use of either Levenberg- Marquardt or

Powell's Dog Leg optimization algorithms, taking as a cost function value of the reprojection error (Eq. 12) [7].

$$\epsilon = \sum_i d(x_i, \bar{x}_i)^2 + d(x_i', \bar{x}_i')^2 \tag{12}$$

where $\bar{x}_i = P_1 x_i$, $\bar{x}_i' = P_2 x_i'$ and $d(\cdot)$ is a Euclidean distance.

The outcome is refined projection matrix and 3D points locations (stage f). This usual approach was mentioned in [8, 9].

Scene reconstruction leaves many aspects of potential enhancement, and so, Chao Zhang et al. introduced a modified feature descriptor (based on Local Binary Patterns) for acceleration and accuracy improvement of stereo matching [10]. On the other hand, Marek Kowalski and Władysław Skarbek made use 4D subspace tracking procedure so that noise during key-points detection could be reduced [11]. Other authors focused on providing more dense (with more points) reconstruction with depth camera [12] or prior sparse representation [13, 14]. In the method presented in this paper, we focused on providing more accurate reconstruction within shorter processing time. In our method, an additional step, called **outliers rejection** (stage e'), was introduced into algorithm flow (see Fig. 3). Many authors focus on outliers rejection only as a result of 2D RANSAC procedure for features matching while still many poorly fitted points may be left within inliers set. Besides that, the new cost function, defined as **relative reprojection error** (ϵ^R), was set in the non-linear optimization procedure for bundle adjustment. Also, for needs of bundle adjustment process, Jacobian matrix was estimated using, more accurate, central difference.

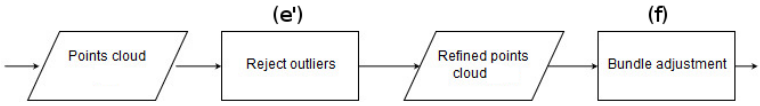

Figure 3: Proposed extension of the scene reconstruction procedures. Source: Own work

3. Method

Standard reprojection error (Fig. 4) is a distance between feature originally detected in an image (x_j), and its triangulated 3D counterpart (Y_j) projected ($\bar{x}_j$)

onto the image plane with estimated projection matrix ($\mathbf{P_2}$) of the camera with the center at the point O (Fig. 4). Due to noise and error cumulation, the points x_j and $\bar{x_j}$ rarely overlap. Leaving it as it is may result in reasonably disturbed 3D model structure. However, absolute value of the error may decide about model uselessness to be not necessarily right, since it ought to be referred to some scale.

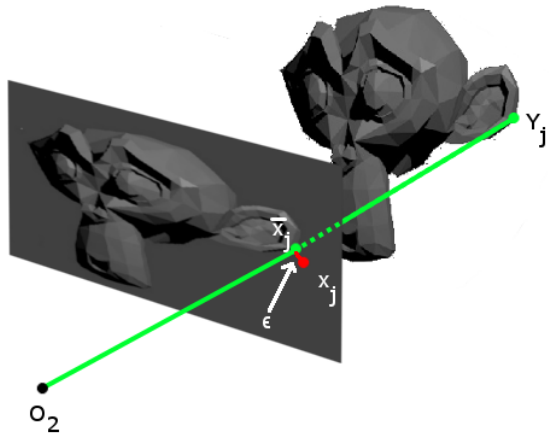

Figure 4: Visualization of the reprojection error. Source: Own work

Relative reprojection error ϵ^R (Eq. 13) is a new measure of reconstruction quality with respect to reconstructed model projection. It is a relative quantity which associates value of reprojection error with height and width of frames being processed.

$$\epsilon^R = \sum_{j=1}^{n} d\left(\frac{d_m^x(x_j, \bar{x_j})}{W} \cdot 100\%, \frac{d_m^y(x_j, \bar{x_j})}{H} \cdot 100\%\right) \text{ subject to } \bar{x_j} = P_2 x_j \qquad (13)$$

where $d(\cdot)$ is a Euclidean distance is a Euclidean distance; W is an image width; H is an image height; $d_m^x(\cdot)$ is a Manhattan distance along horizontal axis; $d_m^y(\cdot)$ means a Manhattan distance along vertical axis; x_j is a 2D feature; $\bar{x_j}$ is a 2D point created as a projection of a 3D counterpart (Y_j) by the projection matrix P_2; n is a number of all points correspondences

Below in the chapter 3, successive stages of the reconstruction algorithm are presented together with the additional step introduced in this paper.

3.1. Feature extraction

Both frames being processed need to be described by features which can be detected quick and which may be matched precisely afterwards. King and Panchal suggests SIFT, ORB or SURF features to be suitable for this purpose[15], nevertheless SIFT features are significantly slower than the others. Concerning time comparison between ORB and SURF the authors were not able to present authoritative results because of some unknown errors. Due to the fact that only SURF features gained a point for detection speed, and there is no strong emphasis on the huge number of features, we used this kind of descriptor in the reconstruction process (for comparison tables, see [15]). The SURF features detected on a single image of the monkey, may be seen in the Figure 5.

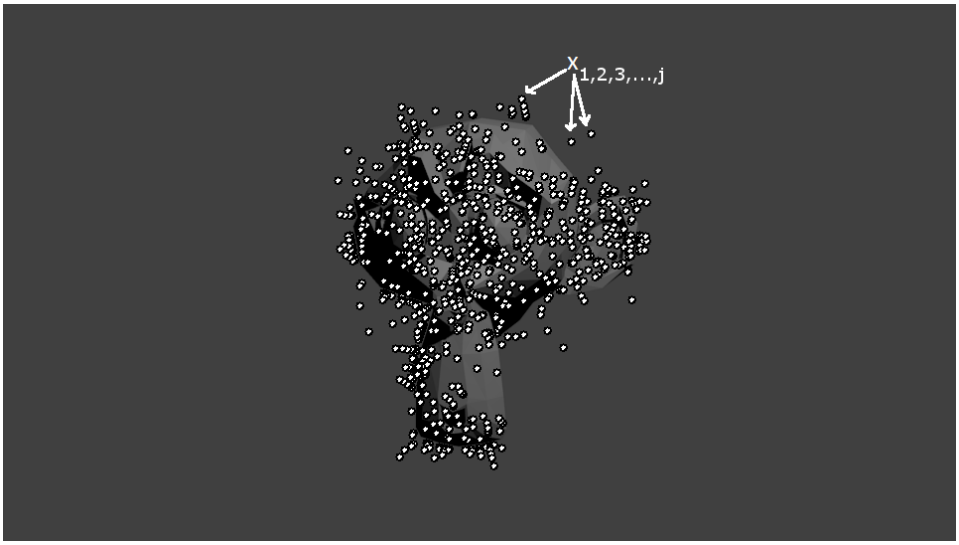

Figure 5: SURF features detected onto the subject. Source: Own work

3.2. Correspondence searching

Searching for matches among 2D features is the widely elaborated topic in the literature of the subject. The benchmark method for SURF features, presented in [16], uses features vectors of the length of 64 bytes so as to speed up matching and keeping enough distinctiveness, and robustness. Even though, simple descriptors matching might result in many mis-correspondences (see Fig. 6).

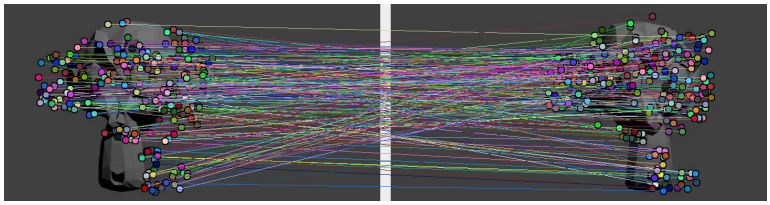

Figure 6: SURF features matched in the two frames. Source: Own work

To prevent influence of mismatches onto the final result, the method of random sample consensus (RANSAC) was employed. Though it consumes additional time (see section 4), it improves much final result by rejection of matches which do not fit the model (are too far in the other image after transformation) (see Fig. 7). We may notice that all matches represent, approximately, the same transformation unlike in the Figure 6.

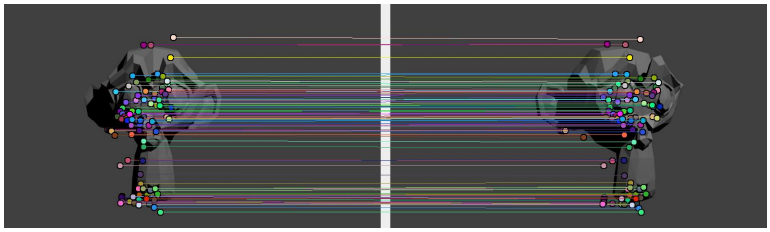

Figure 7: SURF features matched with RANSAC method. Source: Own work

3.3. Camera projection matrix estimation

Camera projection matrix were approximated based on inliers found with RANSAC method. The core of calculation is finding the solution of the 8-point algorithm, formulated as in the Equation 14

$$\mathbf{Ae} = \begin{bmatrix} x_{1,x}x'_{1,x} & x_{1,x}x'_{1,y} & x_{1,x} & x_{1,y}x'_{1,x} & x_{1,y}x'_{1,y} & x_{1,y} & x'_{1,x} & x'_{1,y} & 1 \\ \vdots & \vdots & \vdots & \vdots & \vdots & \vdots & \vdots & \vdots & \vdots \\ x_{j,x}x'_{j,x} & x_{j,x}x'_{j,y} & x_{j,x} & x_{j,y}x'_{j,x} & x_{j,y}x'_{j,y} & x_{j,y} & x'_{j,x} & x'_{j,y} & 1 \end{bmatrix} \begin{bmatrix} e_1 \\ e_4 \\ e_7 \\ e_2 \\ e_5 \\ e_8 \\ e_3 \\ e_6 \\ e_9 \end{bmatrix} = 0 \tag{14}$$

where $\mathbf{A}$ is a composition of points coordinates in the reference and the control frame, and $\mathbf{e}$ is a column-wise flatten vector of an essential matrix entries (Eq. 2).

Unfortunately, due to noise, the matrix $\mathbf{A}$, of Singular Value Decomposition of the form $\mathbf{A} = \mathbf{UDV^T}$, does not have rank 8 and the exact solution is not defined. But one may find the exact solution of $\hat{\mathbf{A}}\mathbf{e} = 0$ which minimizes the Frobenius norm to $\mathbf{Ae} = 0$ [7]. Then, using singular value decomposition, we may find $\hat{\mathbf{A}}$ as $\hat{\mathbf{A}} = \mathbf{U}\hat{\mathbf{D}}\mathbf{V^T}$ where $\hat{\mathbf{D}}$ is $\mathbf{D}$ (matrix with singular values on diagonal) with the last (smallest) singular value set to zero.

Afterwards, by solving camera ambiguity problem (i.e. choosing one out of four projection matrix for which all (or most) points lie in front of both cameras, see subsection 2) we obtain camera projection matrix $\mathbf{P_2}$ as transformation including information about the rotation and translation of cameras coordinate systems.

3.4. Triangulation

Thanks to triangulation, 3D points' counterparts (Y_j) may be found by seeking for the point in between two back-projected rays going through the camera origins and locations of the feature in both frames (see Fig 8).

3.5. Outliers rejection

Even the very first step of reconstruction pipeline may produce errors which are propagated and accumulated in successive stages, making significant impact onto the final result. Mis-localized keypoints or mis-matched correspondences are only cases in point. In order to diminish their influence, a process of initial refinement has been introduced in this paper. Contrary to bundle adjustment, which

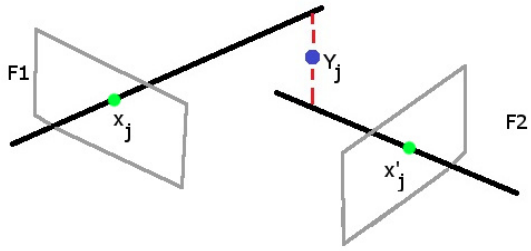

Figure 8: Visualization of triangulation process. Source: Own work

usually improves extrinsic camera parameters (or 3D locations) explicitly [17, 18], initial refinement works indirectly operating on the features.

The sense of outliers rejection is to reject outlying key-points, thus features whose ϵ^T takes the highest and the lowest values. Statistically, the trimmed mean enables describing well an overall data tendency [19]. If contribution of extreme measurements is high, arithmetical average may be, at least, misleading.

Obviously, the width of the rejection border ought to be adjusted bearing in mind the trade-off between structure completeness and structure accuracy. In our research, structure completeness is measured as the total surface of a mesh constructed with Delaunay triangulation. Hence, we are looking for the optimum rejection border such that error decrease is low and total surface is preserved high.

3.6. Bundle adjustment

The fundamental process of bundle adjustment procedure is Jacobian matrix calculation in the discrete domain. We have applied central difference (Eq. 15) for derivatives estimation, since it provides better accuracy in comparable time than backward or forward distance.

$$f'(x) = \frac{f(x+h) - f(x-h)}{2h} \tag{15}$$

For optimization process we tested two algorithms: Levenberg- Marquardt and Powel's DogLeg. The latter works faster and provides similar results, thus we decided to apply that one. Into the core optimization algorithm, Powel's DogLeg suggested in [20], we have introduced a modification in the form of Jacobian matrix approximation by central difference calculation; and applying value of ϵ^R as a

Table 1: Intrinsic parameters used for tests

Parameter name	**Value**
focal length (f_x)	1050
focal length (f_y)	1050
principal point (c_x, c_y)	(480.0, 270.0)
skew	0.0

cost function (Eq. 13).

4. Tests and Results

In the testing process we have evaluated reconstruction of four distinguished objects of different complexity (see Fig. 9): the polyhedron (42 vertices), the monkey (507 vertices), the dragon (22,126 vertices) and the car (31,020 vertices). We opted synthetic models so as to avoid problem and inaccuracies involved with camera parameters and calibration. Having chosen projections of ready model, we posses accurate intrinsic camera parameters (Tab. 1) built into the application.

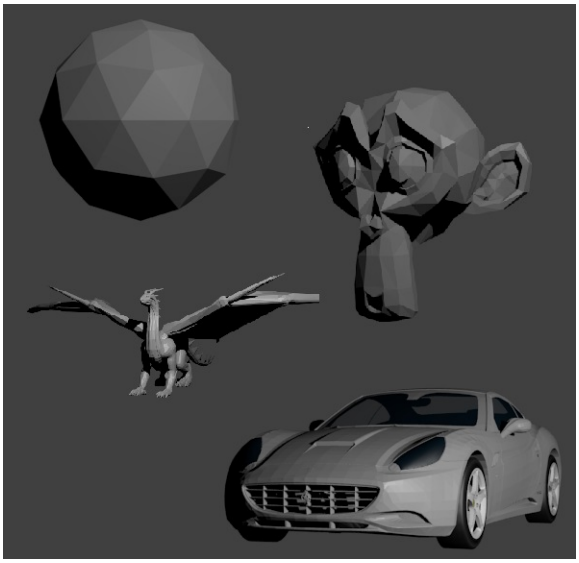

Figure 9: Subjects being evaluated during the testing stage. Source: Own work

Prior to evaluation of proposed modifications, the proper value rejection border need to be selected. The Figure 10 presents dependency between fall of ϵ^R in % and rejection border width in %, and between value of the total mesh surface and rejection border. We may notice that dependency has logarithmic character, thus

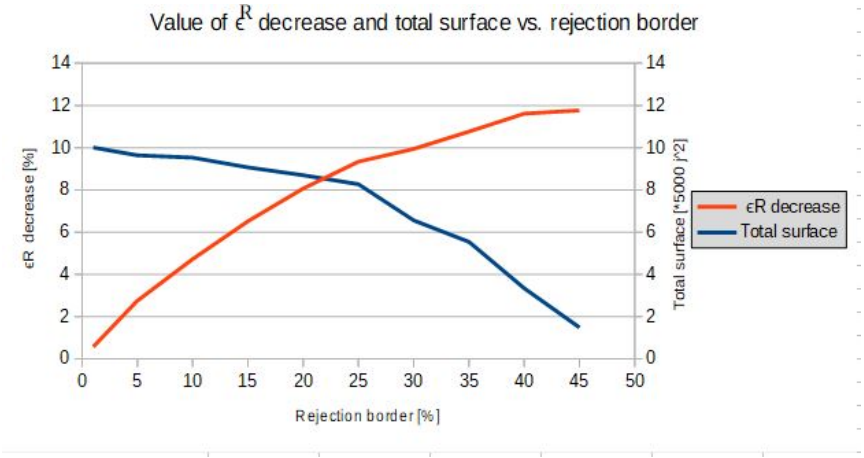

Figure 10: Value of ϵ^R decrease and value of the total surface with respect to rejected points part

value of actual accuracy gain is lower and lower. Although, the width of rejection border is customizable parameter fitting to the problem, Wilcox recommends general value of 20% [21]. In the Figure 10 we may notice that desired width of the rejection border is between 20% and 25%. These values assure high ϵ^R decrease preserving still much information about the structure (expressed by the sum of surfaces of triangles of the object's mesh). In our considerations we have taken the width of 20% for our tests.

The charts below (Fig. 11) depict values of ϵ^R for standard reconstruction pipline and for reconstruction flow with the proposed modifications. Values are represented with respect to the initial object's complexity expressed by a number of its vertices.

As it may be noticed, values of ϵ^R for the suggested changes are lower and have shorter lower and upper bounds for confidential level of $\rho = 0.95$, than for the usual approach. It should be observed that error decrease, supplied by the introduced modifications, is gained regardless of a model's complexity.

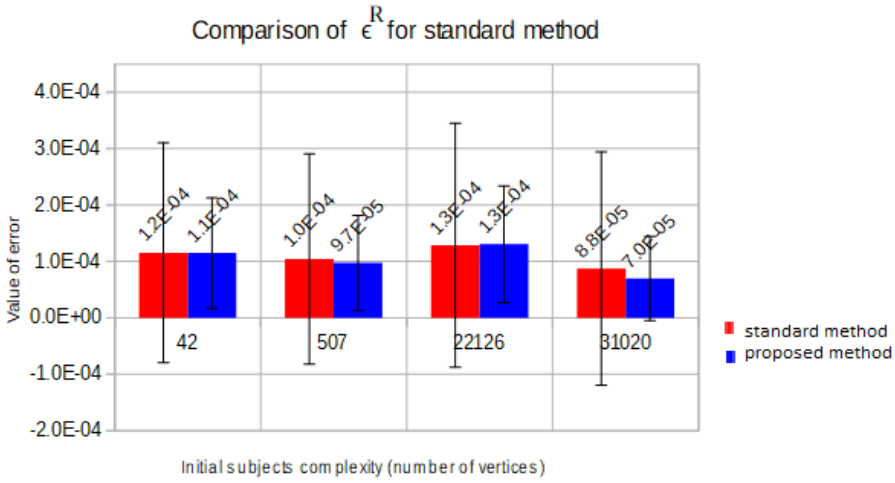

Figure 11: Value of average ϵ^R for standard (red) and proposed (blue) method with confidential level $\rho = 0.95$

The successive chart (Fig. 12), in turn, shows maximal values of the relative reprojection error for standard and proposed method. Undoubtedly, value of maximum error (associated with the worst reconstructed point) is significantly lower by applying our improvements. Moreover, value of maximal error for conventional approach increases steadily, whereas for our method it fluctuates and tends to decrease.

Reprojection statistics are crucial, but particular attention ought to be paid also to execution time. It is presented in the Figure 13 as a juxtaposition of time for the reference and the suggested method. The proposed method tends to keep constant reconstruction time regardless of initial subject's complexity, whereas for the standard approach, time values vary significantly.

5. Conclusions

In this paper modifications of the benchmark two-view reconstruction process was presented, namely, extension of the procedure by additional step of extrema rejection and application of the Relative Reprojection Error (ϵ^R)as a cost function for bundle adjustment DogLeg algorithm, instead of ordinary reprojection error.

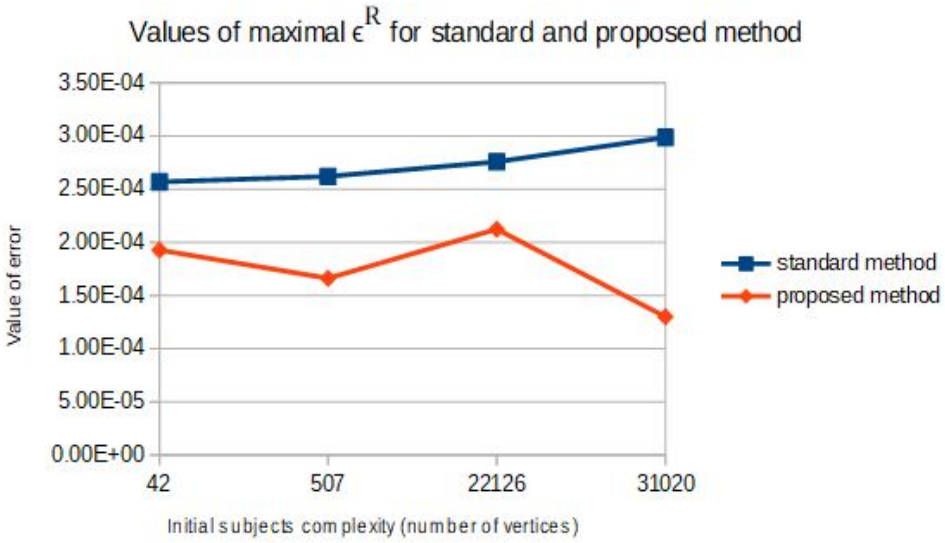

Figure 12: Value of maximal ϵ^R

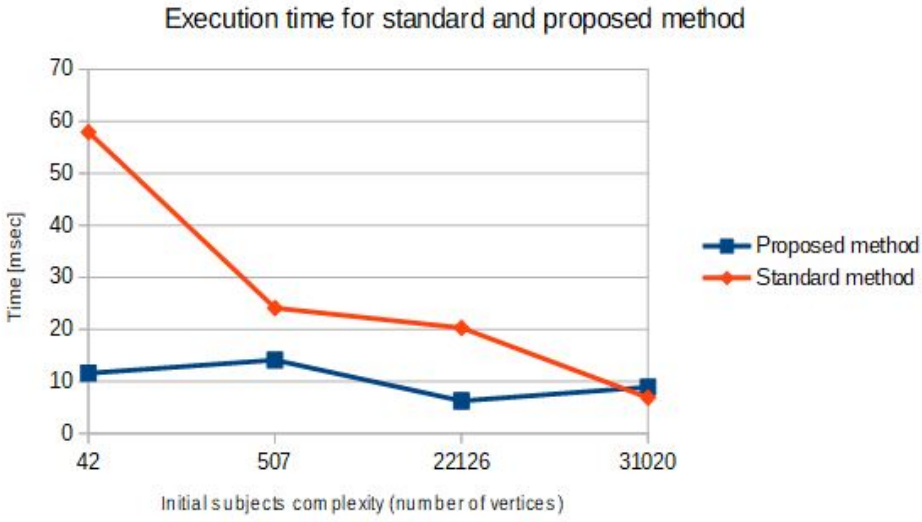

Figure 13: Execution time for standard and proposed method

Both changes influenced results of test, providing better reprojection statistics in shorter processing time. Further research in this topic should be led towards update the suggested method to the incremental reconstruction pipline and time reduction for real-time application.

References

[1] Megyesi, Z., *Dense Matching Methods for 3D Scene Reconstruction from Wide Baseline Images*, Ph.D. thesis, Eotvos Lorand University, 2009.

[2] Izadi, S., Kim, D., Hilliges, O., Molyneaux, D., Newcombe, R., Kohli, P., Shotton, J., Hodges, S., Freeman, D., Davison, A., and Fitzgibbon, A., *KinectFusion: Real-time 3D Reconstruction and Interaction Using a Moving Depth Camera*, In: Proceedings of the 24th Annual ACM Symposium on User Interface Software and Technology, UIST '11, ACM, New York, NY, USA, 2011, pp. 559–568.

[3] Mertz, C., Koppal, S. J., Sia, S., and Narasimhan, S. G., *A low-power structured light sensor for outdoor scene reconstruction and dominant material identification*, In: 9th IEEE International Workshop on Projector-Camera Systems, Pittsburgh, PA, June 2012.

[4] Zhao, H. and Shibasaki, R., *Reconstructing a textured CAD model of an urban environment using vehicle-borne laser range scanners and line cameras*, Machine Vision and Applications, Vol. 14, No. 1, apr 2003, pp. 35–41.

[5] Yang, Y. Q., Xiao, Q., and Song, Y. H., *The investigation of 3D scene reconstruction algorithm based on laser scan data*, In: 2010 International Conference on Machine Learning and Cybernetics, Vol. 2, July 2010, pp. 819–823.

[6] Roman, Z., Evgeny, P., and Dmitry, S., *Structured Light + Range Imaging. Lecture 17*, 2012, Lecture notes.

[7] Hartley, R. and Zisserman, A., *Multiple View Geometry in Computer Vision*, chap. 4, Cambridge University Press, 2nd ed., 2003, p. 108.

[8] Westoby, M., Brasington, J., Glasser, N., Hambrey, M., and Reynolds, J., *'Structure-from-Motion' photogrammetry: A low-cost, effective tool for geoscience applications*, Geomorphology, Vol. 179, No. Supplement C, 2012, pp. 300 – 314.

[9] Micheletti, N., Chandler, J. H., and Lane, S. N., *Structure from Motion (SfM) Photogrammetry*, British Society for Geomorphology, 2015.

[10] Zhang, C., Xue, B., and Zhou, F., *Low-dimension local descriptor for dense stereo matching and scene reconstruction*, Optical Engineering, Vol. 56, No. 08, aug 2017.

[11] Kowalski, M. and Skarbek, W., *Online 3D face reconstruction with incremental Structure From Motion and a regressor cascade*, Vol. 9290, 2014, pp. 9290 – 9290 – 8.

[12] Asif, U., Bennamoun, M., and Sohel, F., *Simultaneous dense scene reconstruction and object labeling*, In: 2016 IEEE International Conference on Robotics and Automation (ICRA), IEEE, Stockholm, Sweden, may 2016.

[13] Lari, Z. and El-Sheimy, N., *A new approach for progressive dense reconstruction from consecutive images based on prior low-density 3D point clouds*, Vol. XLII-2/W7, Wuhan, China, sep 2017.

[14] Kowalczyk, M., Fornalczyk, K., Napieralski, P., and Staniucha, R., *Computer Game Innovations*, chap. Disparity detection in three-dimensional scenes implementing virtual reality, LODZ UNIVERSITY OF TECHNOLOGY PRESS, 2016.

[15] King, A. and Panchal, J., *Analysis of Keypoint Detection Algorithm for Space - Based SFM*, Tech. rep., Spring, 2017.

[16] Bay, H., Tuytelaars, T., and Van Gool, L., *SURF: Speeded Up Robust Features*, Springer Berlin Heidelberg, Berlin, Heidelberg, 2006, pp. 404–417.

[17] Gong, Y., Meng, D., and Seibel, E. J., *Bound constrained bundle adjustment for reliable 3D reconstruction*, Opt. Express, Vol. 23, No. 8, Apr 2015, pp. 10771–10785.

[18] Agarwal, S., Snavely, N., Seitz, S. M., and Szeliski, R., *Bundle Adjustment in the Large*, In: Eleventh European Conference on Computer Vision (ECCV 2010), Springer Verlag, October 2010.

[19] Little, T. D., *The Oxford Handbook of Quantitative Methods: Foundations*, Vol. 1, chap. Robust Statistical Estimators, Oxford University Press, 2013.

[20] Madsen, K., Nielsen, H., and Tingleff, O., *METHODS FOR NON-LINEAR LEAST SQUARES PROBLEMS*, Technical University of Denmark, 2nd ed., apr 2004.

[21] Wilcox, R. R., *Introduction to robust estimation and hypothesis testing*, Elsevier Academic Press, 2005.